

Quantitative U/Th deposition and cleanliness control strategies in the JUNO site air

Jie Zhao,^{1,*} Chenyang Cui,^{1,2} Yongpeng Zhang,¹ Gaosong Li,¹ Nan Wang,¹ and Monica Sisti³

¹*Institute of High Energy Physics, Chinese Academy of Sciences, Beijing, China*

²*University of Chinese Academy of Sciences, Beijing, China*

³*Istituto Nazionale di Fisica Nucleare - sezione di Milano Bicocca,
piazza della Scienza 3, I-20126 Milano, Italy*

The Jiangmen underground neutrino observatory (JUNO) is made of a 20 kt liquid scintillator (LS) detector at a depth of 700 m underground. In order to meet all physics requirements, the $^{238}\text{U}/^{232}\text{Th}$ content in the LS is required to reach a level of 10^{-17} g/g. However, the radioactivity of dust in the air is about 12 orders of magnitude higher than that, so there is an extremely high requirement for the cleanliness of the installation environment on site. In this study, a clean room management mode was implemented in the 120,000 m³ space of the JUNO underground experimental main hall, to control the environmental cleanliness at a level equivalent to a class 10,000-100,000 clean room. Additionally, we designed a method to directly measure the deposition rate of $^{238}\text{U}/^{232}\text{Th}$ on the surface of the detector. Based on ICP-MS detection, the sensitivity to $^{238}\text{U}/^{232}\text{Th}$ concentrations can reach the level of picograms (pg). This helps to implement the cleanliness control strategies and to assess the level of external contamination during the construction of the detector.

arXiv:2507.05759v1 [physics.ins-det] 8 Jul 2025

* zhaojie@ihep.ac.cn

I. Introduction

Dust in the air typically contains radioactive $^{238}\text{U}/^{232}\text{Th}$ at the level of ppb-ppm. Therefore, for ultra-low background detection technology and low-background experiments, there are strict requirements for environmental cleanliness. The underground rock at the Jiangmen Underground Neutrino Observatory (JUNO) site contains 9.6 ppm of ^{238}U and 26.6 ppm of ^{232}Th [1]. The walls of the experimental hall have only been sandblasted and not specially protected, allowing rock powder to disperse into the air and settle onto the surface of the detector during construction activities and ventilation.

The main target medium of the JUNO experiment is a 20 kt liquid scintillator (LS) contained in a 35.4 m diameter acrylic sphere. To meet all JUNO physics requirements, the $^{238}\text{U}/^{232}\text{Th}$ content in the LS is required to reach a level of 10^{-17} g/g, which is about 12 orders of magnitude lower than the $^{238}\text{U}/^{232}\text{Th}$ content in the rock, thus imposing extremely high cleanliness requirements on the detector and its surroundings. Additionally, if too much dust accumulates on the outside of the acrylic sphere, the gamma radiation resulting from $^{238}\text{U}/^{232}\text{Th}$ decay in the dust can penetrate the water layer (see Figure 1) and contribute to the background of the LS. This necessitates stringent cleanliness requirements not only for the acrylic vessel containing the LS but also for the entire installation environment in the hall.

Furthermore, in an environment which requires a certain level of cleanliness, it is necessary to quantitatively measure how much natural radioactive $^{238}\text{U}/^{232}\text{Th}$ will settle on the detector. Inductively Coupled Plasma Mass Spectrometry (ICP-MS) has extremely high sensitivity for measuring $^{238}\text{U}/^{232}\text{Th}$, allowing for the design of experiments to quantitatively measure the actual $^{238}\text{U}/^{232}\text{Th}$ deposition rate under known levels of environmental cleanliness. This work will provide a detailed overview of the cleanliness control strategies implemented at the JUNO site and the current level of cleanliness achieved.

The structure of the article is as follows: Section II describes the detector construction in the JUNO experimental hall, Section III describes the cleanliness control indicators at the JUNO site, Section IV presents the cleanliness control strategies and the long-term cleanliness monitoring results in the hall, Section V describes the experiments and results of $^{238}\text{U}/^{232}\text{Th}$ deposition rates in the air based on ICP-MS, and Section VI presents the application to JUNO, Section VII is the summary of this work.

II. Overview of the JUNO detector

The conceptual design of the JUNO detector is illustrated in Figure 1. A 20 kt LS, serving as the target for neutrino detection, is contained within a 35.4-meter-diameter acrylic sphere. The entire acrylic sphere is supported by a 41.1-meter-diameter Stainless Steel (SS) truss, which is held in place by SS support rods. A total of 17,612 20-inch and 25,600 3-inch Photomultiplier Tubes (PMTs) are installed on the SS truss, designed to detect the faint light signals generated by neutrino interactions with the LS. The entire spherical structure is housed within a cylindrical cavity measuring 43.5 m in diameter and 44 m in height. This cavity is filled with 40 kt of ultra-pure water, which, in combination with the top-mounted track detector, serves to mark cosmic rays and

shield against environmental background. Additionally, magnetic shielding coils are installed on the SS truss to mitigate the interference of the Earth’s magnetic field on the PMTs. A calibration room is positioned at the top of the spherical detector, approximately 9 meters above the surface of the acrylic sphere. Due to the lower density of the LS compared to water, the liquid level inside the acrylic sphere is maintained 4.5 m higher than the external water level to ensure pressure equilibrium. Consequently, a 9-meter chimney extends upward from the top of the acrylic sphere. To account for light blocking, mechanical strength, and background effects, the lower 1 m section of the chimney is made of acrylic, while the remaining portion is constructed of stainless steel. The chimney’s upper end extends into the top calibration room, allowing calibration sources to be introduced into the detector’s interior through the chimney for calibration purposes.

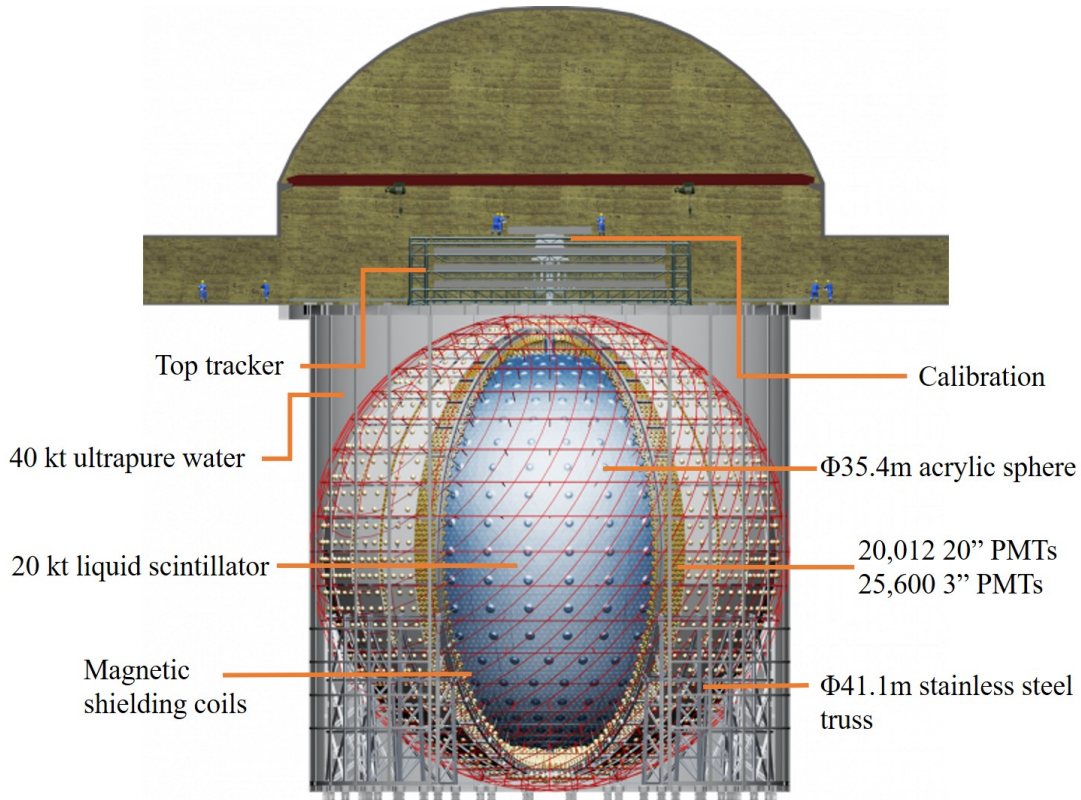


FIG. 1. Conceptual diagram of the JUNO detector.

III. Cleanliness requirement

JUNO high-purity scenario requires the $^{238}\text{U}/^{232}\text{Th}$ concentration in its 20 kt LS to be at the level of 10^{-17} g/g, corresponding to a maximum of 0.2 μg for both ^{238}U and ^{232}Th . After the completion of the detector construction, the JUNO acrylic sphere will first be filled with Ultra-Pure Water (UPW) from the bottom, then the LS will be injected from the top to replace the UPW inside the sphere. During the filling process, the air inside the sphere will come into direct contact with the acrylic surface and the UPW. The most conservative assumption is that all the

dust in the air inside the sphere will be transferred to the LS. The dust in the air mainly comes from rock powder, with a radioactive assumption consistent with that of the rock (9.6 ppm ^{238}U and 26.6 ppm ^{232}Th). Therefore, it is required that the dust content in the air be less than 8 mg, dominated by ^{232}Th concentration. According to the particle size distribution in the cleanroom, assuming that the particles are spherical and their density is similar to the rock of 2.6 g/cm^3 , the total particle mass in a cleanroom of class 1,000 * is 12 mg, which is close to the requirement for the LS. During the actual filling process, the air inside the sphere will be vented from the top, and the dust in the air will not all settle on the water and acrylic surfaces. However, we conservatively require the cleanliness of the air inside the sphere to reach class 1,000 before filling it with water.

The space of the JUNO experimental main hall is approximately $120,000\text{ m}^3$, and it is difficult to control the cleanliness level of such a large space within the class 1,000 standard. Therefore, after the construction of the acrylic sphere, the upper and lower chimney openings were temporarily sealed with a plate to avoid significant exchange of internal and external gases. The inner surface of the acrylic sphere was protected by a film during the construction process. The main material of this film is paper, with one side coated with a thin layer of water-soluble adhesive. During the final cleaning process, the adhesive dissolves, allowing the paper film attached to the surface of the organic glass to naturally fall off. Therefore, before removing the protective film, it is possible to use 3D nozzles to generate micron-level water mist, allowing the dust in the air inside the sphere to adhere to the water droplets and settle to the bottom of the acrylic sphere, thereby further improving the air quality inside the sphere. Based on usual observations, the concentration of particulate matter in urban air significantly improves immediately after rain, typically reducing by one order of magnitude. With better optimization and design at JUNO site, we expect the effect of dust reduction through water mist in the 35.4 m diameter acrylic sphere allows an improvement of one to two orders of magnitude in the cleanliness. Therefore, we require the initial state inside the sphere – that is, in the installation environment – to reach a cleanliness level of class 10,000-100,000 in the installation environment of the hall.

The dust deposited on the outer surface of the acrylic sphere, PMT, and stainless steel (SS) truss during the construction process, can produce gamma rays by the natural radioactivity inside. The gamma rays can penetrate through the water layer and the acrylic sphere and enter the LS, constituting the background. Based on the JUNO software framework [2], we simulated the natural radioactivity on the outer surface of the acrylic sphere, PMT, and the SS truss [3]. The probability for the deposited energy of being greater than 0.7 MeV and be positioned within the fiducial volume ($R < 17.2\text{ m}$) of the LS for each natural radioactive nuclide is listed in Table I. Taking the acrylic outer surface as an example, 1 Bq of ^{238}U will lead to 0.001 Hz event rate in the LS with deposited energy larger than 0.7 MeV at a position with radius smaller than 17.2 m, while the rate is one order of magnitude larger for ^{232}Th , which has more energetic gamma rays in the chain (^{208}Tl). At the same time, the radon produced by ^{238}U in the dust will enter the shielding water, causing an increase of radon concentration. The background impact of the outer detector requires knowledge of the $^{238}\text{U}/^{232}\text{Th}$ settling rate of the dust in the air. To this aim, we designed an experiment to expose containers and pads, with extremely low background levels, to a known cleanliness environment for a certain period of time. We then measured the $^{238}\text{U}/^{232}\text{Th}$ content

* A class 1,000 environment is equivalent to ISO class 6 according to "Federal Standard 209E".

deposited on the surface of the containers and pads using ICP-MS. The experimental details and results will be presented in detail in Section V.

TABLE I. Based on the JUNO software framework, we simulated the natural radioactivity on the outer surface of the acrylic sphere, PMT, and the SS truss. The gamma rays produced by the decay of natural radioactivity can penetrate through the water layer and acrylic sphere and ultimately enter the LS. The probability of deposited energy being greater than 0.7 MeV and position within the fiducial volume ($R < 17.2$ m) of LS from each radioactivity is listed in the table.

		Acrylic outer surface	PMT&Truss
Radius [m]		17.8	19.2-20.0
Probability	^{238}U	1.1×10^{-3}	3.4×10^{-6}
	^{232}Th	1.3×10^{-2}	1.4×10^{-5}
	^{40}K	1.1×10^{-3}	1.3×10^{-7}

IV. Cleanliness control strategies

A. Overall environment

In early 2022, the SS truss construction began in an installation environment that was still very poor at that time. The hall and ancillary rooms were not sealed and were connected to the outside traffic support tunnel. The rock walls inside the hall were only sandblasted, without any other special protection. There were four fume hoods in the hall with a circulation and filtration capacity of 200,000 m³/h to improve the cleanliness of the hall. The weathered rock powder on the surface of the rock walls would float into the air with the airflow, and the activities of the installation personnel would also bring dust. The air cleanliness was at a level of class 1,000,000.

In order to improve the cleanliness of the hall environment, we carried out a deep cleaning of the hall in April 2022. The rock walls above the ground level of 3 m were cleaned with water to reduce dust caused by personnel activities. For areas above 3 m, water flushing was challenging on one hand, and the ducts had sponges and could not be flushed with a large amount of water. However, it is believed that with long-term circulation and filtration, the dust that can be carried away by the airflow will gradually decrease. All surfaces such as the floor, handrails, and ducts were vacuumed and then wiped again. The walls of the cylindrical water pool, with a diameter of 43.5 m and height of 44 m, were rinsed with deionized water, and the installed SS structure was also rinsed with deionized water.

The cargo shower rooms at the top and bottom entrances of the hall were completed and put into operation in early May 2022. From then on, all goods and personnel entering the hall needed to pass through the air shower to remove surface dust. In the same month, fire doors were installed in the ancillary rooms around the hall, effectively achieving isolation between the hall and the outside traffic support tunnel. At the same time, we set up dressing areas at the entrances of the two cargo shower rooms to implement a clean room management mode in the hall. Personnel entering the hall needed to change into special anti-static clean suits in this area. Plastic mats were

laid on the cement floor inside the hall to facilitate cleaning and reduce dust caused by personnel movement on the cement floor.

In early July 2022, the SS truss was completed, and preparations were made to begin the assembly of the acrylic sphere. Prior to this, we carried out a second cleaning of the truss, using vacuum cleaners for dust removal and wiping with a damp cloth. At the same time, we inspected the rusting situation in certain areas of the SS truss, and treated the rust spots by removing the rust and applying polyurea protection.

The acrylic sphere has the highest cleanliness requirement. Therefore, starting from the installation of the acrylic sphere, we have implemented strict cleanroom management in the experimental hall. The main measures are as follows:

- All personnel entering the hall must wear dedicated cleanroom suits, hats, and shoe covers.
- All goods and equipment entering the hall must be cleaned outside the hall, wrapped in protective film during transportation, and the film must be removed at the hall entrance and passed through the air shower in the cargo shower room before entering the hall.
- The paper outer packaging of all goods and equipment must be removed at the entrance of the cargo shower room before entering, and only low-dust paper boxes customized by PMT are allowed to enter.
- Components waiting for installation in the hall must be stored on dedicated plastic trays isolated from the ground, and the surface of the components must be covered with anti-static clean cloth for protection. All tools or small installation components in the hall must be placed in dedicated plastic boxes and covered with clean cloth for protection.
- Welding and cutting operations are not allowed in the entire hall and the surrounding traffic support tunnel.

In terms of management, the overall communication and coordination are the responsibility of the head of the background task force, the heads of the various subsystems are responsible for review and implementation, and the quality inspection is carried out by the gatekeeper.

We conducted cleanliness level measurements at multiple points inside the hall and found that the differences were minimal. This is because a circulating purification fan with a capacity of 200,000 m³/h is operating in the hall, which results in a relatively uniform distribution of particulate matter in the air. Therefore, we selected a fixed point within the hall for long-term stability testing. The long time monitoring of cleanliness inside the hall is shown in Figure 2. Some key clean control measures have been marked in the figure. According to the particle size distribution in the class 10,000 environment (ISO class 7), all particles can be calculated as spherical to obtain the total particle volume per unit volume of air at the class 10,000 level. We continuously monitor the particle size distribution in the air inside the hall using a laser dust particle counter and calculate the real-time total particle volume per unit volume based on spherical particles. The values on the Y-axis in the graph represent the real-time total particle volume divided by the total particle volume at the class 10,000 level, indicating the cleanliness level relative to the class 10,000 level. With all of the efforts described above, the cleanliness inside the experimental hall has reached the

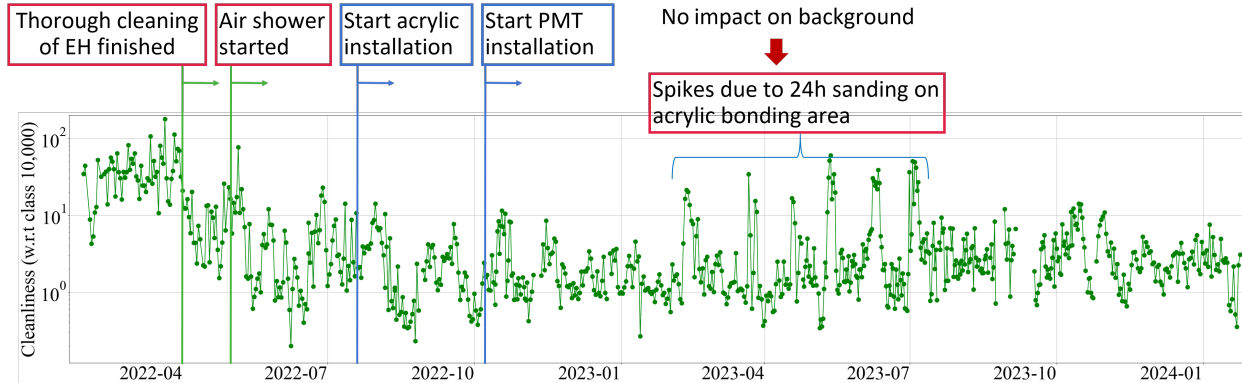


FIG. 2. The long time monitoring of cleanliness inside the hall, as well as some key clean control measures are shown in the figure. Some of the larger peaks from March to July in 2023 mainly resulted from the dispersion of acrylic powder into the air during the polishing of the acrylic panel joints.

equivalent of a class 10,000-100,000 level since May 2022, with an average cleanliness level of class 74,000. The 35.4 m diameter acrylic sphere is assembled on-site with 265 acrylic panels, with each layer being meticulously polished to improve its smoothness. Starting in 2023, the installation of acrylic increased the number of construction workers, and the installation schedule was changed to two shifts per day. Some of the larger peaks from March to July in the graph mainly resulted from the dispersion of acrylic powder into the air during the polishing of the acrylic panel joints. During non-polishing periods, the cleanliness level in the hall mostly remains at class 10,000. Since the acrylic material we used to build the acrylic sphere was very clean – less than 10^{-12} g/g measured U/Th concentrations, the acrylic powder generated during the polishing process has minimal impact on the background compared to rock dust.

B. Detector cleaning and protection

The SS truss installation of the JUNO detector was finished in June 2022: the truss then underwent three extensive cleanings in 2022, including water flushing and wiping processes. Moreover, before installing each of the PMT layers, we conducted another thorough cleaning of the corresponding area in the SS truss.

The installation of the acrylic sphere began in July 2022 and was completed by the summer of 2023 at the equatorial layer, with the lower hemisphere installation completed in October 2024. The outer surface of the acrylic sphere was covered with a protective film throughout the installation process. Unlike the film attached to the inner surface, the film on the outer surface is made of polyethylene with a minimal amount of regular adhesive on one side. This film requires manual removal, and laboratory tests have confirmed that the residual background impact of the adhesive is negligible. From September to October 2024, we completely removed the protective film, cleaned the acrylic outer surface using a clean cloth, and painted the seam with epoxy. The inner surface of the acrylic sphere was also protected by another type of film during the construction process, which was ultimately removed by final 3D high-pressure spraying inside the sphere.

The mass installation of PMTs started in early 2023 and reached the equatorial layer by April

2024, with the completion of the lower hemisphere installation in December 2024. In February 2024, we cleaned the surface of the installed PMT area with an electrostatic duster.

V. U/Th settling measurement

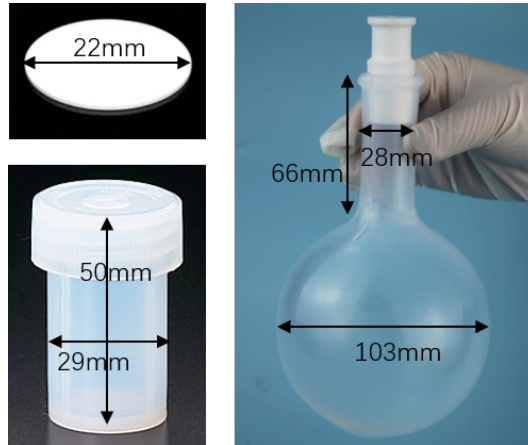


FIG. 3. Sampling plate and vessels. The total sampling areas are 4 cm^2 , 60 cm^2 , and 390 cm^2 for the PTFE and acrylic plate, PFA cylindrical container, and PFA flask, respectively.

We have designed three sampling methods, namely PTFE and acrylic plate, PFA cylindrical container, and PFA flask, as shown in Figure 3. Given that containers made of PFA material typically exhibit an extremely low background, they are well-suited for ultra-low concentration U/Th measurements when combined with ICP-MS. Therefore, in this experiment, PFA flasks were used to simulate the shape of acrylic sphere, aiming to compare the U/Th deposition rates with those of other shapes. To match the sample processing containers, sampling plates were custom-made only in PTFE and acrylic materials. These were used to compare the U/Th deposition rates between acrylic and PTFE, which, to some extent, reflects the differences in deposition rates on the surfaces of PFA and acrylic glass materials.

The plate is placed in different orientations (upward, downward, and sideways) to compare the U/Th settling rates in different directions. The idea of this measurement is similar to that carried out at Pacific Northwest National Laboratory (PNNL) and the SNOLAB underground facility [4]. The PFA cylindrical container simulates the settling rate on the surface of a cylindrical detector, while the PFA flask simulates the settling rate on the surface of a spherical detector, which is the form of the JUNO acrylic sphere. All the sampling plate and containers underwent the following rigorous cleaning process to minimize the external contamination:

- Degreasing: all sampling plates and containers are soaked in a 0.1% Alconox solution and sonicated for 5 min, followed by rinsing with deionized water, then sonicated in deionized water for another 5 min.
- Primary acid washing: the sonicated sampling plates and containers are placed in an acid tank containing 20% GINUIS nitric acid and soaked overnight.

- Secondary acid washing: after being removed from the acid tank and rinsed with deionized water, the sampling plates and containers are boiled in 20% GINUIS nitric acid for 30 min and then rinsed with deionized water.

A. Sampling

The PTFE and acrylic plates are fixed on a dust-free plastic pad with needles, with 15 plates in one group. Among them, 12 plates are stacked in pairs to simulate the sampling surfaces facing upwards and downwards, while the remaining three plates are placed sideways. This arrangement ensures that each sampling point has a sampling area of 23 cm² in three different orientations, as shown in Figure 4.(1). Both the PFA flat-bottomed bottle and PFA flask are sampled with the bottle cap open, with both the bottle mouth and the cap facing upwards or downwards (Figure 4.(2)). To investigate whether there are differences in the settling of U/Th in open and closed spaces, we created a simple small cover and placed the PFA sampling bottles inside the cover for sampling, comparing it with the sampling bottle outside the cover (Figure 4.(2)). There are a total of four sampling points in the JUNO underground experimental halls, including the top hall, the PMT and acrylic interlayer (Figure 4.(3)), the acrylic installation platform (Figure 4.(4)), and the installation space outside the main hall. Each sampling point is equipped with three types of sampling containers and a particle size analyzer (Lighthouse Handheld 3016), which is used for continuously monitoring the particle size distribution.

B. Sample treatment process

The acrylic sphere was assembled in the JUNO experimental hall by bonding it layer by layer. After each layer of acrylic is assembled, the seams need to be polished to improve the smoothness. During the polishing process, a large amount of acrylic powder is generated, which floats in the air and is collected by our containers. Therefore, the sample treatment process not only requires the use of acid to dissolve the inorganic salts, but also requires the removal of the acrylic powder inside through filtration or ashing methods.

For the PTFE and acrylic plates, the size can fit into a 23 mL PFA cylindrical bottle, so the sampling and sample processing are both done in the PFA cylindrical bottle. The sample treatment process for all samples is as follows:

- Add 4 mL (20 mL) of 5% nitric acid (Fisher Scientific) and 0.5 g of hydrofluoric (HF) acid (Fisher Scientific) to a 23 mL PFA cylindrical bottle (500 mL PFA flask), and heat it for 25 minutes. The purpose of adding HF acid here is to dissolve any silicates that may be present in the sample.
- For the plates, after acid boiling, the plate is removed and rinsed with 1 mL of hot 5% nitric acid to ensure that any residual sample solution on the plate is also washed off.
- Remove organic powder: in order to remove the acrylic powder from the acid solution, the acid solution needs to be filtered or ashed. For the filtration method, all acid solutions are

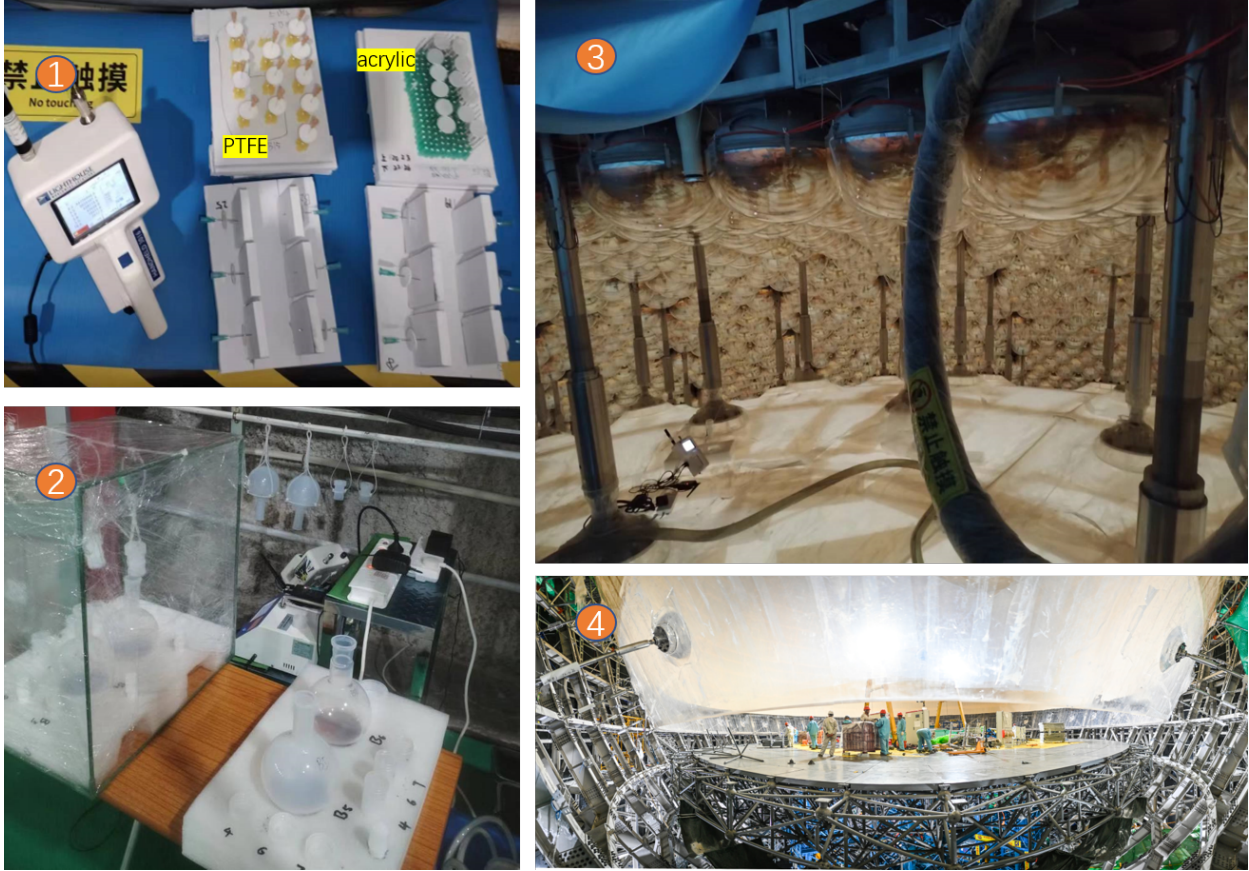


FIG. 4. Some sampling pictures in JUNO experimental hall. Figure 1 and Figure 2 depict the sampling photographs taken from the installation room and the hall floor, respectively. Figure 3 shows the sampling image captured between the layers of acrylic sphere and the PMT. Figure 4 illustrates the installation platform for the acrylic sphere, where we conducted our sampling.

drawn into a syringe and filtered through a filter with a $0.2\ \mu\text{m}$ aperture, and heating to dry to remove HF acid (because HF acid can corrode the ICP-MS), then 2 g of 20% nitric acid is added and heated to dissolve the residual; for the ashing method, all acid solutions are transferred to a platinum crucible, placed in a muffle furnace, and completely ashed at a temperature of 600°C , then 5 g of 20% nitric acid is added and heated to dissolve the inorganic residue in the platinum crucible. We got similar results from these two ways of treatment, so we chose filtration for future samples.

- Measurement: after the acid is made up to volume, the sample is sent for ICP-MS measurement.

C. Blanks and recovery efficiency

The blank experiment involves repeating all the pre-treatment processes for the samples, the only difference being that no sample is added. The blank results can be used to evaluate the level of external contamination in the entire pre-treatment process. The blank results of the pre-treatment

process are summarized in Table II. The PTFE is not so clean as PFA, so the blanks are above 1 pg with relatively larger standard deviation (SD). The method detection limit (MDL) at 99% confidence level (C.L.) is calculated as $\bar{X} + t \times SD$, where \bar{X} is the average blank on U/Th, t -value relies on the number of replicates [5]. From the results, it can be seen that the U/Th blanks of 23 mL PFA bottle, 500 mL flask, and platinum crucible after acid boiling and filtration operations are 0.2-0.6 pg, while the blanks of PTFE and acrylic plate acid boiling and ashing are 1-2 pg.

Vessel	Pre-treatment	Parallels	^{238}U [pg]			^{232}Th [pg]		
			\bar{X}	SD	MDL	\bar{X}	SD	MDL
23 mL PFA bottle	acid heating+filter	24	0.2	0.1	0.4	0.2	0.1	0.4
500 mL PFA flask	acid heating+filter	16	0.3	0.1	0.6	0.5	0.2	0.9
Platinum crucible	acid heating+ashing	9	0.4	0.3	1.3	0.6	0.3	1.6
PTFE plate (6 pieces)	acid heating+filter	10	0.8	0.4	2.0	1.1	0.7	3.0
Acrylic plate (6 pieces)	acid soaking+filter	8	1.5	0.6	3.3	2.2	1.7	7.3

TABLE II. Blank results for different treatments.

The entire pre-treatment process's U/Th recovery efficiency was determined by adding known amounts of naturally non-existent ^{229}Th and ^{233}U standards (preserved in 5% nitric acid) to the samples, subjecting them to the same pre-treatment process, and finally sending them for ICP-MS testing. The measurement results of 10 samples showed U/Th average recovery efficiency around 106%/108%, with a standard deviation of 5%, as shown in Figure 5. The possible reason for a recovery rate exceeding 100% is that the sampling and sample processing containers are reused in the laboratory. During the sample processing, U/Th elements can permeate into the container walls and also leach out from them. After the cleaning procedure described in Section VB, the containers reach an equilibrium between the permeation and leaching processes during sample handling. This equilibrium is corrected for the ratio of ^{232}Th and ^{238}U by using the recovery rates of ^{229}Th and ^{233}U .

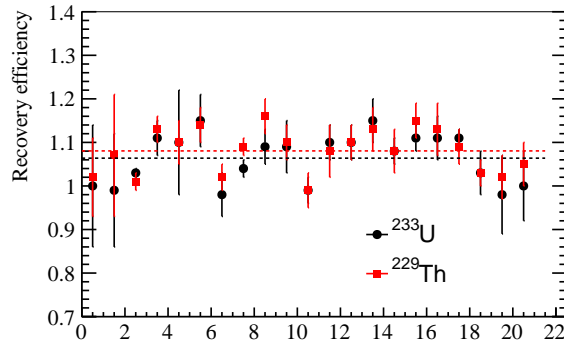


FIG. 5. The U/Th recovery efficiency for the entire pre-treatment. The average efficiencies of ^{233}U and ^{229}Th are shown in the black and red dash line.

D. Results

Outside the JUNO underground experimental hall, there is an installation room with a cleanliness level of class 40,000-50,000. The measurement data collected from all sampling containers placed at the same location (installation room) are presented in Table III, aiming to eliminate the interference of acrylic powder in the experimental hall. From the results in the table, the following conclusions can be drawn:

- The settling rate of U/Th in open spaces (No.2 and No.5) is about two orders magnitude higher than in closed spaces (No.1 and No.4);
- The settling rate of U/Th in spherical flasks (No.5) is about six times lower than in cylindrical containers (No.2);
- For cylindrical bottles (No.2 and No.3) and spherical flasks (No.5 and No.6), the settling rate of U/Th with the mouth of the bottle facing upwards is 30-40 times higher than when the mouth is facing downwards.
- The chimney height of the JUNO detector is 9 m, and the diameter of the sphere is 35.4 m. Therefore, the ratio of the chimney height to the sphere diameter is 25%. The ratio of the upper cylindrical section to the lower spherical diameter of the PFA flask is 64%. Concerned about whether the upper straight section might affect the settling inside the sphere, we conducted the following comparative experiment: one original PFA flask and one modified PFA flask with the upper straight section cut down to only 1 cm in height, resulting in a ratio of the upper cylindrical section to the lower spherical diameter of 10%. We compared whether there was any difference in the settling rate at the same position between the original PFA flask and the shortened PFA flask. The results (No. 5 and No. 7) showed that the U/Th sedimentation outcomes of both flasks were consistent within the uncertainty.
- The deposition amount of U/Th on the upper surface of the PTFE plate (No.8) is similar to that on the acrylic plate (No.11), but the results show that the deposition amount on the lower surface (No.9) or side (No.10) of the PTFE plate is 4 or 5 times higher than that of the acrylic plate (No.12 and No.13). The deposition on the upper surface is a combination of dust settling and adsorption processes. From the results, the deposition on the upper surface is primarily due to gravitational settling of dust, while the deposition on the lower surface or side is mainly attributed to adsorption.

At about the same time, we placed the sampling bottles and particle counting machine at different locations within the JUNO experimental hall, and left them collect the dust with the same exposure period settled for the outside installation room. The measured settling rates of U/Th and cleanliness levels are summarized in Table IV.

From the results of the cylindrical container, the U/Th settling rates in the Top hall (No. 1) and the acrylic installation platform (No. 3) are similar; however, the air particle counting differ by an order of magnitude. This discrepancy is due to the fact that the acrylic installation process involves polishing the surface of the bonding area, resulting in a significant amount of acrylic powder that

TABLE III. All sampling containers are placed at the same location (in the installation space outside the JUNO underground experimental hall with cleanliness level of class 40,000-50,000) for 12-14 days in May-Sep 2024, and the measured settling rates are summarized in the table. The average value and the standard deviation among three parallels samples are shown in the last column. The PFA flask with label "1 cm" represents the modified PFA flask with the upper straight section cut down to only 1 cm in height.

No.	Vessel	Space	Direction	Settling [pg/d/m ²]	
				²³⁸ U	²³² Th
1	PFA bottle	closed	upwards	<3.0	<3.6
2		open	upwards	280±15	438±26
3		open	downwards	10±2	12±2
4	PFA flask	closed	upwards	<0.7	<1.0
5		open	upwards	51±14	73±23
6		open	downwards	4±1	2.0±0.6
7	PFA flask (1 cm)	open	upwards	43±17	54±26
8	PTFE plate	open	upwards	1624±232	1869±67
9		open	downwards	394±169	504±345
10		open	sideways	406±98	371±25
11	Acrylic plate	open	upwards	1166±442	1809±887
12		open	downwards	24±6	93±83
13		open	sideways	157±60	98±9

TABLE IV. Sampling was conducted using the same type of sampling bottle and facing upwards at different locations for 9-14 days in April-Sep 2024, and the measured cleanliness levels (measured by the particle counting machine) and corresponding U/Th settling rates are summarized in the table. The average value and the standard deviation among three parallels samples are shown in the last column.

No.	Vessel	Location	Cleanliness [×10 ⁴]	Settling [pg/d/m ²]	
				²³⁸ U	²³² Th
1	PFA bottle	Top hall	4.8	691±60	926±26
2		Interlayer	13	397±11	445±71
3		Platform	216	657±72	804±49
4		Installation hall	3.8	280±15	438±26
5	PFA flask	Top hall	4.8	67±43	77±48
6		Interlayer	13	34±11	34±19
7		Installation hall	3.8	51±14	73±23

interferes with the measurement of airborne dust particle sizes. The U/Th settling rates in the acrylic and PMT interlayers are close to those measured outside the hall, likely because there is less human activity in this area compared to the Top hall and installation platform. For the flask container, the geometric effects lead to a settling rate that is nearly an order of magnitude lower

than that of the cylindrical container.

VI. Application to the JUNO detector systems

We plan to evaluate the potential U/Th deposition on the surfaces of acrylic sphere, PMTs, and the SS truss during the installation process, based on the U/Th deposition rate measurements from the previous section. This will allow us to assess the impact of contamination from these detector surfaces on single-event rates in the LS after the detector is completed. As shown in Table III, for flat plates made of PTFE and acrylic, the results for the upward-facing orientation are quite similar. Although there are differences in the results for the downward-facing and side-facing orientations, their contributions are relatively minor compared to the upward-facing results. A similar trend is observed for PFA cylindrical bottles and flasks. This indicates that gravitational settling of dust during environmental exposure plays a dominant role. Therefore, even though the previous experiments did not simulate all detector material types, we can still refer to the results from PFA cylindrical bottles and flasks when evaluating deposition rates. Since the aforementioned detector structures are uniformly spherical, we intend to use the measurement results from PFA flasks for background evaluation. Additionally, the 20 kt LS, which has been purified through a four-stage purification system and filled into acrylic sphere via a filling system, requires assessment of U/Th deposition on the surfaces of LS-contacting systems (such as pipes and containers) due to environmental exposure during installation. These systems are mostly cylindrical, so we plan to use the measurement results from PFA cylindrical containers for background evaluation. Based on the estimated U/Th deposition on detector surfaces during construction, we will further calculate the impact of these natural radioactivities on single-event rates in the LS, as well as the levels of ^{238}U -induced radon contamination in water from water-contacting detector structures.

A. Acrylic inner surface

After the acrylic sphere was constructed, a 3D spray head was placed into the sphere from the top. The first step is to spray water mist to reduce the dust particle content inside the sphere, with a cleanliness improvement to class 1,000 level. The second step involves high-pressure water flushing of the inner surface of the acrylic sphere to remove the surface protective film and perform the final cleaning. After these two steps, the cleanliness levels at various heights within the sphere were measured to be in the range of class 100 to 1,000. Upon completion of the cleaning process, the upper chimney was sealed with an acrylic blind plate, and the lower chimney was fitted with a stainless steel cover to prevent extensive air exchange between the interior and exterior of the sphere. Subsequently, the remaining 8-meter section of the stainless steel chimney and the calibration room were installed. Each section was sealed with nitrogen gas after installation. Once the calibration room was fully installed, the blind plate on the upper chimney was removed, and nitrogen gas was circulated through the chimney to maintain a positive pressure within both the upper chimney and the calibration room.

The total area of the acrylic inner surface amounts to 4,000 m². The acrylic filling process involves initially filling the inside and outside of the sphere with ultra-pure water, then displacing

the ultra-pure water with LS inside the sphere. The entire time for cleaning took 15 days, and after additional 15 days for chimney and pipes installation, we started the water filling of the vessel on Dec 18, 2024. Based on the experimental results from the previous section, the settling rate of U/Th in spherical flasks during exposure in a closed space and controlled environment of class 1000 is estimated to be lower than $0.02 \text{ pg/m}^2/\text{d}$, assuming a linear change in settling rate with cleanliness and similar U/Th settling on PFA flask and acrylic sphere. Therefore, the estimated U/Th settling during the one month exposure before filling (assuming a cleanliness of class 500-5,000) is of about 1.3-13 ng. During the filling process, the acrylic sphere and water surface were also exposed to air, but the exposed acrylic surface would change with the filling process. The entire filling process took two months, and the average acrylic surface exposure is one month due to the filling process. Therefore, the estimated U/Th settling during filling period is similar to that of before filling. Assuming all U/Th settling on the surfaces of the acrylic sphere and water enters the 20 kt LS, it would contribute to $0.13\text{-}1.3 \times 10^{-18} \text{ g/g}$ of U/Th in LS, which is well below our requirement.

One day before the completion of the acrylic sphere cleaning, approximately 6 m^2 (0.15% of the whole acrylic inner surface) of protection film remained attached to the inner surface of the upper hemisphere, as checked by a person from the outer surface of acrylic sphere on Dec. 1st. This is mainly due to the epoxy adhesive at the bonding line potentially sticking to the water-soluble paper while it was not completely dry, resulting in incomplete washing away by the water. Most of the residual paper is located on the upper hemisphere of the sphere, primarily for two reasons: Firstly, during the assembly process of the lower hemisphere, the paper film at the seams is applied in reverse, meaning the adhesive side faces outward to prevent it from bonding with the epoxy. Secondly, all the seams on the lower hemisphere are removed during the final inspection process inside the sphere after its construction. It is worth noting that the amount of residue mentioned here is a rough estimate made by workers through visual inspection, and the results may be slightly exaggerated, as working on the outer surface of the sphere is relatively challenging. The radiopurity of the paper film was screened using a high-purity germanium detector, revealing activity levels of $<0.5 \text{ Bq/kg}$ for ^{238}U (^{214}Pb and ^{214}Bi gammas) and $0.6 \pm 0.2 \text{ Bq/kg}$ for ^{232}Th (^{212}Pb , ^{228}Ac , and ^{208}Tl gammas), based on a 300 g sample. With a density of 47 g/m^2 , a residual of 0.15% (equivalent to 6 m^2) would result in approximately 280 g of film remaining on the inner surface of the acrylic.

To assess the contamination level caused by the water-soluble paper residual upon contact with the LS, we conducted an aging experiment by soaking 25 cm^2 paper film in 60 g LS at 80°C for 24 hours calculated by the Arrhenius equation. This is equivalent to soaking at room temperature (21°C) for 244 days. Subsequently, we measured the U/Th content in the LS before and after soaking by acid extraction and ICP-MS [6]. The results were shown in Table V, and we found that the U/Th leaching effect from the water-soluble paper was at a level of $200\text{-}400 \text{ pg/m}^2/\text{y}$. Considering the 0.15% of paper residual and 20 kt LS mass, the final U/Th extraction from film to LS is $0.6\text{-}1.3 \times 10^{-19} \text{ g/g}$ per year, which is significantly lower than the design specifications. As for the single-event background caused by residual paper left on the acrylic inner surface, the activity is about 0.2 Bq, and this background can be effectively removed through the fiducial volume cut in the analysis.

	Without film [pq]		With film [pg]		Extraction rate [pg/m ² /y]
	No. 1	No. 2	No. 1	No. 2	
²³⁸ U	0.6±0.2	0.9±0.2	5.2±0.8	5.3±0.8	193±21
²³² Th	0.3±0.2	0.7±0.1	12±1	11.0±0.5	420±41

TABLE V. The screening results of U/Th content in the LS before and after film soaking are shown in the table. The U/Th extraction rate in the last column is subtracted blank of U/Th without film soaking.

B. LS purification and filling systems

The JUNO LS is subjected to a sequential four-stage purification process, which includes alumina adsorption, distillation, water extraction, and gas stripping. After this process, it is filled into the acrylic sphere by a filling system. The primary objectives of the alumina and gas stripping systems are to enhance the transparency of the alkylbenzene feedstock and to remove gaseous components from the LS, respectively. Consequently, their capabilities for the purification of U/Th are somewhat limited. The efficiency of the distillation system [7] and water extraction system [8] in removing U/Th impurities is expected to be 99% and 80% respectively. The total inner surface area of the entire system, as well as the surface area weighted by purification efficiency, are summarized in Table VI. With U/Th contamination in the 20 kt LS reaching levels of 10^{-18} g/g, corresponding to a U/Th mass of 20 ng. Therefore, for the 1105 m² inner surface area of the LS-related system, the required U/Th residual should be smaller than 18 pg/m². The U/Th settling rate in class 10,000 environment is estimated at about 400 pg/d/m² based on the results of No.2 PFA bottle facing upwards in Table III, allowing for an exposure time of 65 min in class 10,000 environment. During construction, all interfaces of pipelines and containers are covered with blind plates before docking, and the blind plates are removed during docking. The vast majority of interfaces strictly require an air exposure time during docking of less than 10 min, with internal nitrogen gas protection after docking is completed. Therefore, even if the environmental cleanliness level fluctuates several times higher than the class 10,000 level, the impact of air exposure during the installation of the LS-related system is controllable.

TABLE VI. The weighted surface area considering the 99% and 80% efficiency from distillation and water extraction.

	Surface area [m ²]	Removal eff.	Weighted area [m ²]
Before distillation	2500	99%	25
Before extraction	900	80%	180
After extraction	900	0	900
Total			1105

C. Structure outside the acrylic

The installation situation and progress for acrylic sphere, PMT and SS truss are summarized in Table VII, as well as the expected U/Th settling rate. Details on the construction can be found in Section IV B. The exposure here only include the time after the final cleaning and before filling. The U/Th settling used in the calculation is the results of PFA flask from Table IV during the exposure with the sphere facing upwards (No. 5 for acrylic and truss, No. 6 for PMT layer). The single-event rate within LS from the settled U/Th on the detector surface, and the release of radon in water are listed in the last two rows of the table. Overall, the U/Th contamination introduced during the installation of the detector due to environmental exposure contributes approximately 2 mHz to the single-event rate in the LS fiducial volume ($R < 17.2$ m), accounting for about 0.03% of the total detector contribution (7 Hz [3]). The impact of radon released from the decay of ^{238}U deposited on the detector surface into the water is at a level of 2 mBq/m³ by assuming equilibrium rate as ^{238}U , which is approximately 20% of the water radon target (10 mBq/m³). Additionally, some of the deposited dust can be further purified through the water circulation process.

TABLE VII. The anticipated accumulation of U/Th in the JUNO main detector components is calculated based on exposure time and the results of U/Th fallout measurements. The potential singles rate in the LS fiducial volume (FV, $R < 17.2$ m) and the radon contamination in water are presented in the last two rows.

	Acrylic	PMT	SS truss
Installation start	2022-07	2023-02	2022-01
Install to equator	2023-08	2024-04	2022-04
Installation complete	2024-10	2024-11	2022-06
Final cleaning	2024-09	2024-02	2022-12
Surface area [m ²]	4e3	3e4	1.6e4
Exposure [month]	3	9	24
Settling [pg/m ² /d]	80	35	80
Deposited U/Th [μg]	30	280	920
Singles in FV [mHz]	2	0.03	0.09
Radon in water [mBq/m ³]	0.04	0.4	1.3

VII. Summary

The installation of the JUNO detector spanned three years. To ensure the detector's cleanliness, the on-site installation environment was managed under clean-room conditions, with an average cleanliness level of class 74,000. After the installation of the acrylic sphere and before the filling with LS, the first step of the cleaning involved a water mist dust reduction inside the sphere, which improved the air cleanliness to a level of class 100 to 1,000. The second step involved using a 3D high-pressure nozzle to rinse the inner surface of the acrylic sphere, further enhancing the cleanliness

of the surface in contact with the LS. Surface deposition experiments for U/Th on various containers were conducted in the JUNO experimental hall. Based on the experimental results, the total U/Th deposition during the installation process of the entire detector was evaluated. Through detector simulations, it was determined that the contribution to the single-event rate in the LS fiducial volume is approximately 0.03% of the total rate from detector materials (7 Hz), and the radon contamination in water is at a level of 2 mBq/m³, which is 20% of the requirement (10 mBq/m³).

Acknowledgements

This work is supported by the Youth Innovation Promotion Association of the Chinese Academy of Sciences, CAS Project for Young Scientists in Basic Research (YSBR-099).

-
- [1] Angel Abusleme et al. JUNO physics and detector. *Prog. Part. Nucl. Phys.*, 123:103927, 2022.
 - [2] Tao Lin et al. Simulation software of the JUNO experiment. *Eur. Phys. J. C*, 83(5):382, 2023. [Erratum: *Eur.Phys.J.C* 83, 660 (2023)].
 - [3] Angel Abusleme et al. Radioactivity control strategy for the JUNO detector. *JHEP*, 11:102, 2021.
 - [4] M. L. di Vacri, I. J. Arnquist, S. Scorza, E. W. Hoppe, and Jeter Hall. Direct method for the quantitative analysis of surface contamination on ultra-low background materials from exposure to dust. *Nucl. Instrum. Meth. A*, 994:165051, 2021.
 - [5] United States Environmental Protection Agency 821-R-16-006. https://www.epa.gov/sites/default/files/2016-12/documents/mdl-procedure_rev2_12-13-2016.pdf.
 - [6] Yuanxia Li, Jie Zhao, Yayun Ding, Tao Hu, Jiaxuan Ye, Jian Fang, and Liangjian Wen. A practical approach of measuring 238U and 232Th in liquid scintillator to sub-ppq level using ICP-MS. *Radiat. Phys. Chem.*, 230:112579, 2025.
 - [7] C. Landini et al. Distillation and gas stripping purification plants for the JUNO liquid scintillator. *Nucl. Instrum. Meth. A*, 1069:169887, 2024.
 - [8] Jiaxuan Ye et al. Development of water extraction system for liquid scintillator purification of JUNO. *Nucl. Instrum. Meth. A*, 1027:166251, 2022.